Materials Science in Semiconductor Processing 153 (2023) 107159

Contents lists available at ScienceDirect

Materials Science in Semiconductor Processing

journal homepage: www.elsevier.com/locate/mssp

# Electrical and optical properties and defects of (100)- and (001)-oriented V-doped β-$Ga_2O_3$ crystals grown by EFG

Pengkun Li [a,b], Xueli Han [a,b], Duanyang Chen [a,*], Qinglin Sai [a], Hongji Qi [a,c,**]

[a] Key Laboratory of Materials for High Power Laser, Shanghai Institute of Optics and Fine Mechanics, Chinese Academy of Sciences, Shanghai, 201800, China
[b] Center of Materials Science and Optoelectronics Engineering, University of Chinese Academy of Sciences, Beijing, 100049, China
[c] Hangzhou Institute of Optics and Fine Mechanics, Hangzhou, 311421, China

ARTICLE INFO

*Keywords:*
V-doped β-$Ga_2O_3$
(100) and (001)
Electrical properties
Optical properties
Defects

ABSTRACT

Altering the n-type conductivity and optical properties of ultra-wide bandgap β-$Ga_2O_3$ by impurity doping has been a topic of research interest in the semiconductor field. Simultaneously, β-$Ga_2O_3$ with a monoclinic structure has exhibited interesting anisotropy. In this study, (100) and (001) V-doped β-$Ga_2O_3$ crystals were synthesized by the edge-defined film-fed growth (EFG) method, and their structural, electrical and optical properties, and defects were systematically investigated. V-doped β-$Ga_2O_3$ crystals with a (100) plane have a better crystalline quality and flatter surface than those with a (001) plane. Compared with undoped crystals (~$10^{16}$ $cm^{-3}$), the carrier concentration of the (100) and (001) V-doped β-$Ga_2O_3$ substrates only increased to $4.30 \times 10^{17}$ $cm^{-3}$ and $1.92 \times 10^{17}$ $cm^{-3}$, respectively, which was related to the $V_xO_y$ clusters formed by excess V as trapping traps and the carbon DX center as an electron capture trap formed by the relaxation of C atoms in the direction opposite to that of the C–O bond. The generation of absorption peaks and flat regions in the transmittance spectra was attributed to the introduction of V doping. The etch pit morphology and Raman peak intensity on the surfaces of the (100) and (001) V-doped β-$Ga_2O_3$ substrates were different owing to the anisotropy of the monoclinic lattice structure. These results contribute to the understanding of the influence of V and anisotropy on β-$Ga_2O_3$ crystals and expand their applications in electrical and optical fields.

## 1. Introduction

Semiconductors have driven advances in communications, military systems, transportation, healthcare, and countless other applications [1–7]. Monoclinic beta-gallium oxide (β-$Ga_2O_3$), as a promising ultra-wide bandgap semiconductor material, has attracted extensive attention in recent years owing to its large band-gap (~4.9 eV), high critical breakdown field (~8 MV/cm), and substantially higher Baliga's figure of merit (BFOM, ~3400) compared to SiC and GaN [8]. Additionally, it has a shorter optical absorption edge near 260 nm, located directly in the solar-blind region (<280 nm) [9]. Therefore, β-$Ga_2O_3$ has excellent characteristics and good potential for use in high-power electronic devices and solar-blind ultraviolet (UV) photodetectors [3,10,11].

One of the significant advantages of β-$Ga_2O_3$ when compared to other wide-bandgap semiconductors is that it can grow large and high-quality native substrates from the melt at low cost and high efficiency. At present, growth techniques for bulk β-$Ga_2O_3$ single crystals include the floating zone (FZ) [12,13], Czochralski (CZ) [14,15], vertical Bridgman (VB) [16,17], and edge-defined film-fed growth (EFG) methods [18,19]. Víllora et al. successfully grew β-$Ga_2O_3$ single crystals with diameters of 1 inch in different directions (<100>, <010>, <001>) using FZ and analyzed their stable growth conditions [20]. Galazka et al. reported the growth of 2-inch-diameter β-$Ga_2O_3$ single crystals with a weight of 1 kg by CZ and explored in depth the relationship between large levels of crystal volume (diameter and cylinder length) and oxygen concentration in the growth atmosphere [14]. Hoshikawa et al. prepared β-$Ga_2O_3$ single crystals in ambient air using the VB method for the first time [16] and studied the defects [21]. A β-$Ga_2O_3$ wafer up to 6 inches in diameter was obtained by EFG [22]. Tao et al. obtained columnar β-$Ga_2O_3$ single crystals using the EFG method by introducing a cylindrical Ir die [19,23]. Hence, the EFG technique is an efficient crystal growth method that can grow large and

* Corresponding author.
** Corresponding author. Key Laboratory of Materials for High Power Laser, Shanghai Institute of Optics and Fine Mechanics, Chinese Academy of Sciences, Shanghai, 201800, China.
*E-mail addresses:* chenduanyang@siom.ac.cn (D. Chen), qhj@siom.ac.cn (H. Qi).

https://doi.org/10.1016/j.mssp.2022.107159
Received 18 July 2022; Received in revised form 15 September 2022; Accepted 3 October 2022

special-shaped crystals. It was therefore selected as the growth technology in this study. β-$Ga_2O_3$ single crystals in the (100), (001), and ($\bar{2}$01) directions can be grown by EFG [19,22]. However, the monoclinic crystal structure of β-$Ga_2O_3$ with low symmetry results in physical, electrical, and optical anisotropies. Although the basic physical and optical properties and defects of β-$Ga_2O_3$ crystals in different directions have been characterized and analyzed [17,24–29], research on the electrical and optical properties and defects in different directions is still insufficient owing to the difficulties in growing and processing samples.

The conductivity of β-$Ga_2O_3$ can be regulated by doping with different elements. Effective n-type doping of bulk β-$Ga_2O_3$ has been realized by using shallow donor dopants, including Si, Sn, Cr, Nb, and Ta, and the free electron concentration was in the range of $10^{16} - 10^{19}$ $cm^{-3}$ [12,30–33]. The upper limit of the electron density for Sn-doped β-$Ga_2O_3$ is approximately $2 \times 10^{19}$ $cm^{-3}$, probably because of the high vapor pressure of $SnO_2$ [30]. Nb and Ta with a valence of +5 provided β-$Ga_2O_3$ with more free electrons, bringing their carrier concentrations to $1.8 \times 10^{19}$ and $3.0 \times 10^{19}$ $cm^{-3}$, respectively [12,31]. Furthermore, V belongs to group VB of the periodic table, similar to Nb and Ta. However, there are only a few studies on V-doped β-$Ga_2O_3$. Huang et al. reported on V-doped $Ga_2O_3$ films, and the authors of this paper previously reported on the effect of air annealing on the properties of V-doped β-$Ga_2O_3$ single crystals [34,35]. Therefore, it is essential to study the electrical and optical properties and defects of different V-doped β-$Ga_2O_3$ bulk crystals with different crystal planes.

In this study, the (100) and (001) V-doped β-$Ga_2O_3$ crystals were grown using the EFG approach. The crystallization quality and electrical and optical properties of the (100) and (001) V-doped β-$Ga_2O_3$ crystals and the etch pits introduced by defects are studied and compared. The phenomenon in which the carrier concentration of the β-$Ga_2O_3$ crystals doped with V increased only slightly is explained. The Raman peak intensity and etch pit morphology of the V-doped β-$Ga_2O_3$ crystals with (100) and (001) planes are altered owing to the anisotropy of the monocline structure. The doping of V caused β-$Ga_2O_3$ crystals to be introduced into the absorption peaks and flat regions. These results contribute to a better understanding of the effects of the anisotropy of β-$Ga_2O_3$ crystals and the incorporation of V on their structural, electrical and optical properties, and defects.

## 2. Experimental

### 2.1. Preparation of crystals

2-inch (100) and (001) β-$Ga_2O_3$ slab crystals doped with 0.20 mol% V were grown by the EFG method. Fig. 1 show the schematic of the EFG experimental setup. $Ga_2O_3$ powder (6 N) and $V_2O_5$ powder (4 N) were used as the raw material and dopant, respectively. The mixed source materials ($Ga_2O_3$ and $V_2O_5$) were put into an Ir crucible. A dynamic mixture of 50% Ar and 50% $CO_2$ was utilized as the growth atmosphere. The Ir crucible was heated via multiple coils to a temperature slightly higher than β-$Ga_2O_3$ melting point. After all the source materials were melted, the melt moved upward from the crucible to the upper surface of the Ir die via a slit through capillary action. The β-$Ga_2O_3$ seed crystal then contacted with the melt on the upper surface of the die and initiated crystal growth. The pulling direction of crystal was [010]. The pulling up rate of the crystals was controlled in the range of 5–10 mm $h^{-1}$, and cooled to room temperature at the rate of 20–30 °C $h^{-1}$. V-doped β-$Ga_2O_3$ crystals with two growth planes were successfully grown on the upper surface of the die by controlling the orientation of the crystal using the seed crystal.

### 2.2. Characterization

The crystal structures and qualities of the samples were determined through X-ray diffraction (XRD) using a Bruker D8 ADVANCE X-ray diffractometer (Bruker Corporation, Cu-K$\alpha_1$ radiation; operated at 40 kV and 40 mA; $\lambda = 1.5406$ Å). The surface morphologies of the samples were investigated using a CSPM 5500 atomic force microscope (AFM; China, Karaltay (Beijing) Instruments Co., Ltd.) and a ZEISS LSM900 laser confocal microscope (LCM; Germany, Carl Zeiss AG, Germany). Hall tests were performed at room temperature using an 8404 Hall measurement system (USA, Lake Shore Cryotronics, Inc.). The optical transmittance spectra of the crystals in the wavelength range of 200–2000 nm at room temperature were recorded by a Lambda 1050+ UV/VIS/NIR spectrometer (PerkinElmer Inc., USA). Room-temperature Raman spectra were obtained via an iHR550 spectrometer (Japan, HORIBA, Ltd.) with a 633 nm excitation laser source. The samples were characterized via X-ray photoelectron spectroscopy (XPS) using an ESCALAB 250Xi system (USA, Thermo Fisher Scientific Inc.).

## 3. Results and discussion

### 3.1. Crystal structure

The XRD patterns of (100) and (001) V-doped β-$Ga_2O_3$ crystals are shown in Fig. 2. The highest intensity peaks correspond to the (400) and (002) planes (JCPDF#41–1103), respectively. Higher-order diffraction peaks of the (600), (800), (12 00), and (004) planes were also observed. No impurity peaks were produced by the other orientations. The XRD analysis revealed that the V-doped $Ga_2O_3$ crystals have a monoclinic structure. The crystal with blue peaks belongs to (100)-oriented β-$Ga_2O_3$, and the β-$Ga_2O_3$ crystal with red peaks has a (001) orientation. The diffraction peaks of the (100) and (001) V-doped β-$Ga_2O_3$ crystals shifted slightly toward higher Bragg angles, owing to the small ionic radius of the V ion.

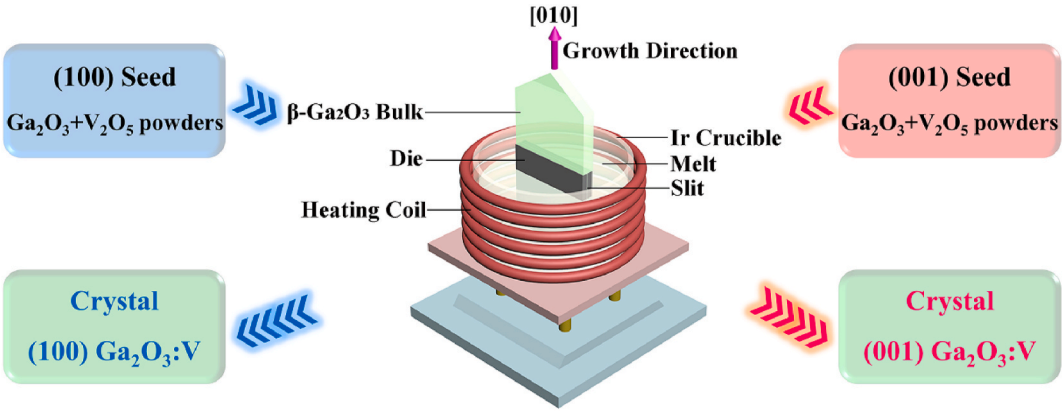


**Fig. 1.** Schematic diagram of the EFG experimental setup for the growth of β-$Ga_2O_3$ crystals.

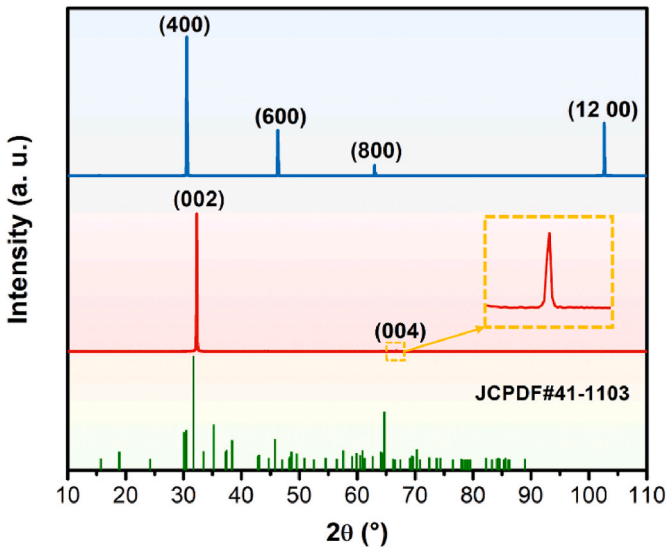


**Fig. 2.** High-resolution XRD patterns of V-doped β-$Ga_2O_3$ crystals.

### 3.2. Crystal quality

The illustrations in Fig. 3 show the (100) and (001) β-$Ga_2O_3$ single-crystal substrates with dimensions of approximately 10 mm × 10 mm (blue and red rectangles), respectively. The crystalline quality of (100) and (001) V-doped β-$Ga_2O_3$ crystals was evaluated using the full-width at half-maximum (FWHM) of X-ray diffraction rocking curve. For the (100) and (001) crystals, the diffraction planes corresponded to the (400) and (002) crystal facets, respectively. The characterization results are shown in Fig. 3. The FWHM values of (100) and (001) V-doped β-$Ga_2O_3$ substrates were 43.2 and 158.4 arcsec, respectively. It is challenging for us to obtain high quality (001) V-doped β-$Ga_2O_3$ crystal due to the growth techniques. The FWHM of the rocking curve of the (001) crystal is nearly four times that of the (100) crystal, indicating that the (100) β-$Ga_2O_3$ crystal has beneficial crystalline quality. In contrast, the poor quality of the (001) crystal is related to internal defects (e.g., dislocations) and stress [36].

Two- (2D) and three-dimensional (3D) surface images of the polished (100) and (001) V-doped β-$Ga_2O_3$ crystals were obtained using AFM, as shown in Fig. 4. The size of the scanning area was 5 μm × 5 μm. The root-mean-square (RMS) roughness values of the (100) (Fig. 4(a) and (b)) and (001) crystals (Fig. 4(c) and (d)) were 0.185 and 0.282 nm, respectively.

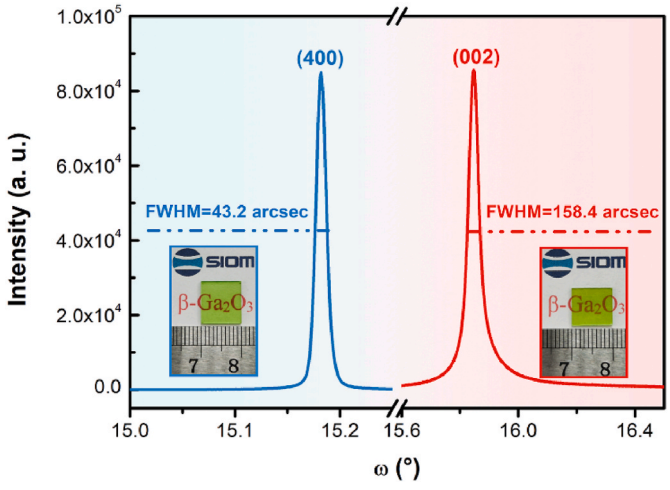


**Fig. 3.** X-ray rocking curves of the (100) and (001)-oriented V-doped β-$Ga_2O_3$ crystals.

Such an ultra-smooth surface indicates that the processing technology for the crystal slab was excellent, which provides a basis for the subsequent preparation of high-performance devices.

### 3.3. Hall characterization

Ti/Al layers with a thickness of 20/100 nm were uniformly sputtered at the four corners on one side of the (100) and (001) V-doped β-$Ga_2O_3$ substrates, as shown in Fig. 5(a). Better ohmic contact of the electrode with the sample surface is a prerequisite for Hall measurement. To improve the ohmic contact behavior, the electrodes (numbered 1, 2, 3, and 4) were annealed at 500 °C for 30 s in an $N_2$ atmosphere. The quality of the ohmic contact can be verified by the current−voltage (*I–V*) characteristics. Fig. 5(c) and (d) show the electrode ohmic contact *I–V* characteristic curves of the (100) and (001) V-doped β-$Ga_2O_3$ substrates, respectively. The current variations between 1 and 2, 2–3, 3–4, and 4–1 were almost linear ($R^2 > 0.9999$) with the applied voltage, indicating that both substrates had ohmic electrodes with excellent contact. However, the *I–V* curves of the four pairs of electrodes (Fig. 5(c) and (d)) show a slight divergence. The divergence may be caused by three factors: (1) electrode quality, (2) sample doping uniformity, and (3) anisotropy of the crystals. As shown from Fig. 5(c) and (d), the quality of the electrodes is satisfactory. Curves 1–2 and 3–4 (as well as curves 2–3 and 4–1) have no anisotropic differences, so that the discretization results from uneven doping. The divergence of 1–2 and 2–3 (3–4 and 4–1) *I–V* behaviors was related to the latter two factors.

The electrical properties of (100) and (001) V-doped β-$Ga_2O_3$ crystals at room temperature are listed in Table 1. The carrier concentrations of (100) and (001) substrates were $4.30 \times 10^{17}$ $cm^{-3}$ and $1.92 \times 10^{17}$ $cm^{-3}$, respectively. The carrier concentration was one order of magnitude higher than that of undoped β-$Ga_2O_3$ crystals (~$10^{16}$ $cm^{-3}$) grown by the EFG technique under the same growth conditions [36], which demonstrated that V acted as a shallow donor to provide free electrons to the β-$Ga_2O_3$ substrates. Nevertheless, compared with β-$Ga_2O_3$ crystals with the same V doping concentration (0.20 mol%, ~$10^{18}$ $cm^{-3}$) grown by the previously reported FZ method [35], the carrier concentration was an order of magnitude lower. In the V-doped β-$Ga_2O_3$ crystals with different concentrations grown by the OFZ method reported previously [37], the carrier concentration ($10^{16}$-$10^{18}$ $cm^{-3}$) increased with the nominal content of V at 0–0.20 mol%. When the nominal composition of V was between 0.20 and 1.0 mol%, the carrier concentration ($10^{18}$-$10^{16}$ $cm^{-3}$) decreased with the increase of V concentration. The samples were tested by ICP, as shown in Table 2. It was found that the actual components of V in 0.2 mol% and 1.0 mol% V-doped β-$Ga_2O_3$ grown by OFZ method were 0.132 and 0.215 mol%, respectively. And the actual contents of V in the (100) and (001) V-doped β-$Ga_2O_3$ samples grown by EFG were 0.177 and 0.185 mol%, respectively, which just fell within the 0.132–0.215 mol% range, so that the carrier concentration was ~$10^{17}$ $cm^{-3}$. This is due to the fact that when the actual content of incorporated V was too high, the excess V formed non-conductive $V_xO_y$ clusters, which acted as traps for capturing electrons [37]. Furthermore, part of C from the growth atmosphere (50% $CO_2$) entering the crystal lattice during crystal growth [38], forming the so-called DX centers that act as compensation acceptors [39]. As shown by theoretical calculations, C prefers to occupy the Ga site in the tetrahedra ($Ga_I$, the β-$Ga_2O_3$ unit cell is shown in Fig. 5(b)), producing a DX center-like behavior in which impurities expected to be shallow donors [40,41] exhibit large lattice relaxation and become negatively charged by trapping electrons, effectively acting as deep acceptors [39]. In addition, we grew (100) V-doped β-$Ga_2O_3$, with residual V in the furnace cavity and the Ir crucible, and then grew (001) V-doped β-$Ga_2O_3$ crystal, so the amount of V in (001) β-$Ga_2O_3$ was higher than (100). The free electron concentration of the (001) crystal was less than that of the (100) crystal, which was caused by more $V_xO_y$ clusters and many defects that acted as traps in the (001) crystal.

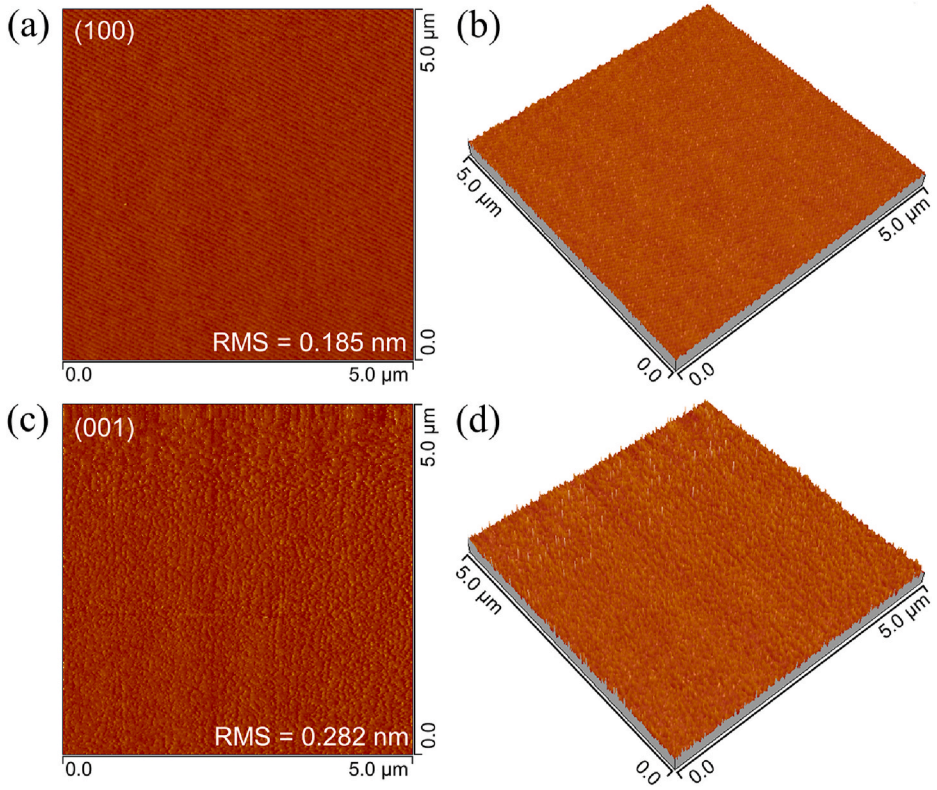


**Fig. 4.** 2D and 3D AFM images of the (100) and (001) V-doped β-$Ga_2O_3$ crystals after polishing.

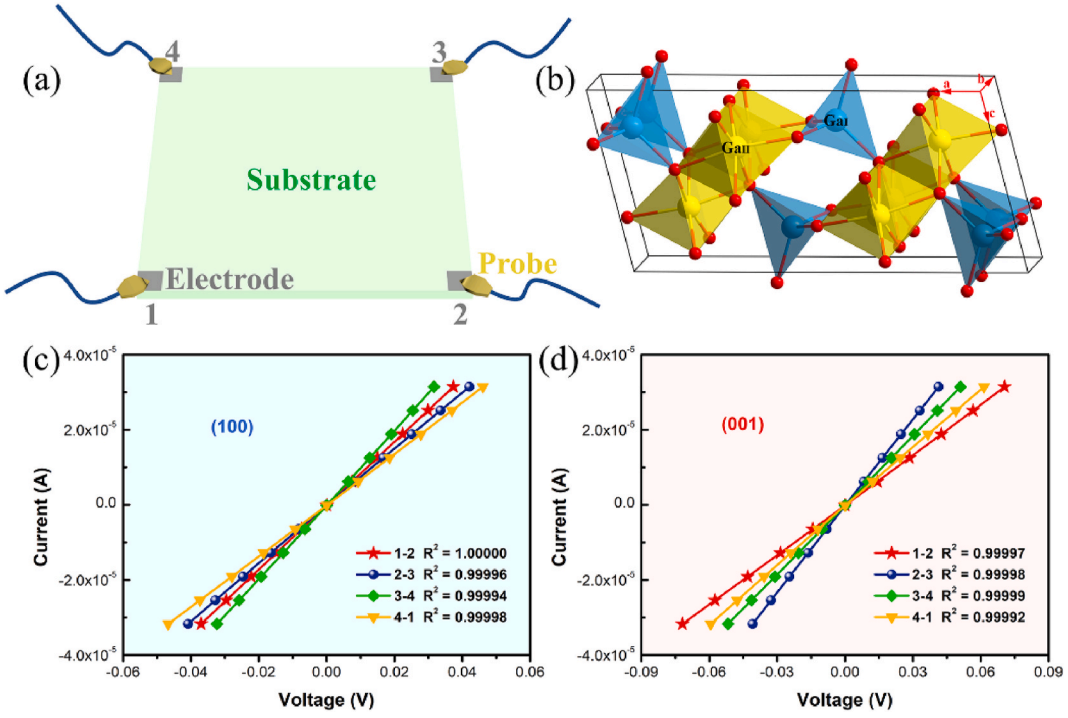


**Fig. 5.** (a) Schematic diagram of Hall effect measurement. (b) Monoclinic structure of the β-$Ga_2O_3$ unit cell. (c and d) *I–V* characteristics of (100) and (001) V-doped β-$Ga_2O_3$ substrates at room temperature.

### *3.4. XPS analysis*

The constituent elements of the (100) and (001) V-doped β-$Ga_2O_3$ crystals were analyzed using XPS. The Ar ion beam was utilized to bombard and clean the crystal surface before the XPS test to minimize the impact of sample surface contamination. Fig. 6(a–c) and (d–f) represent the deconvoluted XPS spectra of C 1s, Ga 3 d-O 2s, and O 1s of the (100) and (001) V-doped samples, respectively. The V characteristic

**Table 1**
Electrical parameters of the (100) and (001) V-doped β-$Ga_2O_3$ single-crystal substrates.

| | Type | Resistivity (Ω·cm) | Mobility ($cm^2$/Vs) | Carrier concentration ($cm^{-3}$) |
|---|---|---|---|---|
| (100) | n | 0.2719 | 54.0 | $4.30 \times 10^{17}$ |
| (001) | n | 0.5786 | 56.0 | $1.92 \times 10^{17}$ |

**Table 2**
ICP results of the V-doped β-$Ga_2O_3$ substrates.

| | Sam.1 (OFZ) | Sam.2 (EFG) | Sam.3 (EFG) | Sam.4 (OFZ) |
|---|---|---|---|---|
| Doping (mol%) | 0.20 | 0.20 | 0.20 | 1.0 |
| ICP (mol%) | 0.132 | 0.177 | 0.185 | 0.215 |

peak could not be captured because the content of V was below the lower limit of the detection equipment. The binding energy scale (284.8 eV) of the C 1s peak was used to calibrate the data.

Fig. 6(a) and (d) show the core level spectra of C1s in (100) and (001) V-doped β-$Ga_2O_3$ crystals. The two primary peaks at 284.79 (Fig. 6(a)) and 284.77 eV (Fig. 6(d)) correspond to C–C bonds [42,43]. The shoulder peaks near 285.61 and 287.60 eV were assigned to C–O and C═O, respectively [42,44], indicating that C in the growth atmosphere entered into β-$Ga_2O_3$ as an impurity and produced C–O and C═O bonds with O, thus being firmly bound within the lattice by O. The relaxation of the C atom towards the interstitial site in the direction opposite to the C–O bond forms a carbon DX center [45]. The lattice relaxation encouraged C to capture free electrons in the β-$Ga_2O_3$ crystals and take negative charges, acting as electron traps [39]. This corresponds to the Hall characterization results.

For the (100) and (001) V-doped samples, the Ga 3 d peaks centered at 20.07 ($Ga^{3+}$, Fig. 6(b)) and 19.90 eV ($Ga^{3+}$, Fig. 6(e)), respectively, are attributed to the Ga bonded to O in $Ga_2O_3$ [46]. The small peaks located at 18.93 (Fig. 6(b)) and 18.84 eV (Fig. 6(e)) are defined as $Ga^{1+}$ [43,46]. The weak and broad peaks located at 22.65 and 22.57 eV are determined to be O 2s [35]. The strong peaks with binding energies centered at 530.76 (Fig. 6(c)) and 530.59 eV (Fig. 6(f)) correspond to O−Ga chemical bonds in $Ga_2O_3$ crystals [47]. The other XPS peaks located at 532.41 (Fig. 6(c)) and 532.22 eV (Fig. 6(f)) are attributed to the O–C bands [43,44], further demonstrating that C enters the lattice of the β-$Ga_2O_3$ crystal to bond with O. The C 1s, Ga 3 d, and O 1s binding energies of the (100) and (001) V-doped β-$Ga_2O_3$ crystals exhibit negligible differences.

### 3.5. Optical properties

The optical transmission spectra of (100) and (001) undoped and V-doped β-$Ga_2O_3$ crystals are shown in Fig. 7. The highest transmittance of the double-sided polished undoped and V-doped β-$Ga_2O_3$ substrates in the visible region was approximately 80% (Fig. 7(a)). However, the introduction of V reduced the transparency in the NIR region. This demonstrates that V provides free electrons to β-$Ga_2O_3$, which is consistent with the Hall characterization results. Interestingly, compared to undoped β-$Ga_2O_3$, the introduction of V results in two additional absorption peaks located at around 400 nm ((100) plane) and 610 nm ((100) and (001) planes). We have previously reported the reason for these two absorption peaks [35]. A small portion of V undergoes a valence state change ($V^{4+}$ and $V^{3+}$) in β-$Ga_2O_3$ [35]. The appearance of the absorption peak was attributed to the crystal field-splitting electron transitions of $V^{4+}$ and $V^{3+}$ [35,48]. Furthermore, it has been reported that there were inherent point defects in β-$Ga_2O_3$, such as self-trapped holes, which acted as deep level acceptors and also leaded to the generation of sub-bandgap absorption peaks at about 400 nm and 610 nm [49]. The absorption peak at approximately 400 nm was not present for the (001) V-doped β-$Ga_2O_3$ substrate, probably because of the anisotropy of the crystal.

Fig. 7(b) shows the transmission spectra of all samples in the range of 200 − 700 nm. The undoped (100) β-$Ga_2O_3$ substrate has one more shoulder than the (001) substrate, which is similar to previous reports [50,51]. Tao et al. [52] characterized the polarized optical transmittance of (100) undoped β-$Ga_2O_3$ crystals. It was found that the transmittances of E//c and E//b were different, contributing to a shoulder corresponding to the transmission of the unpolarized (100) plane [52]. It is worth noting that V doping not only introduced absorption peaks, but also produced a flat region for both the (100) and

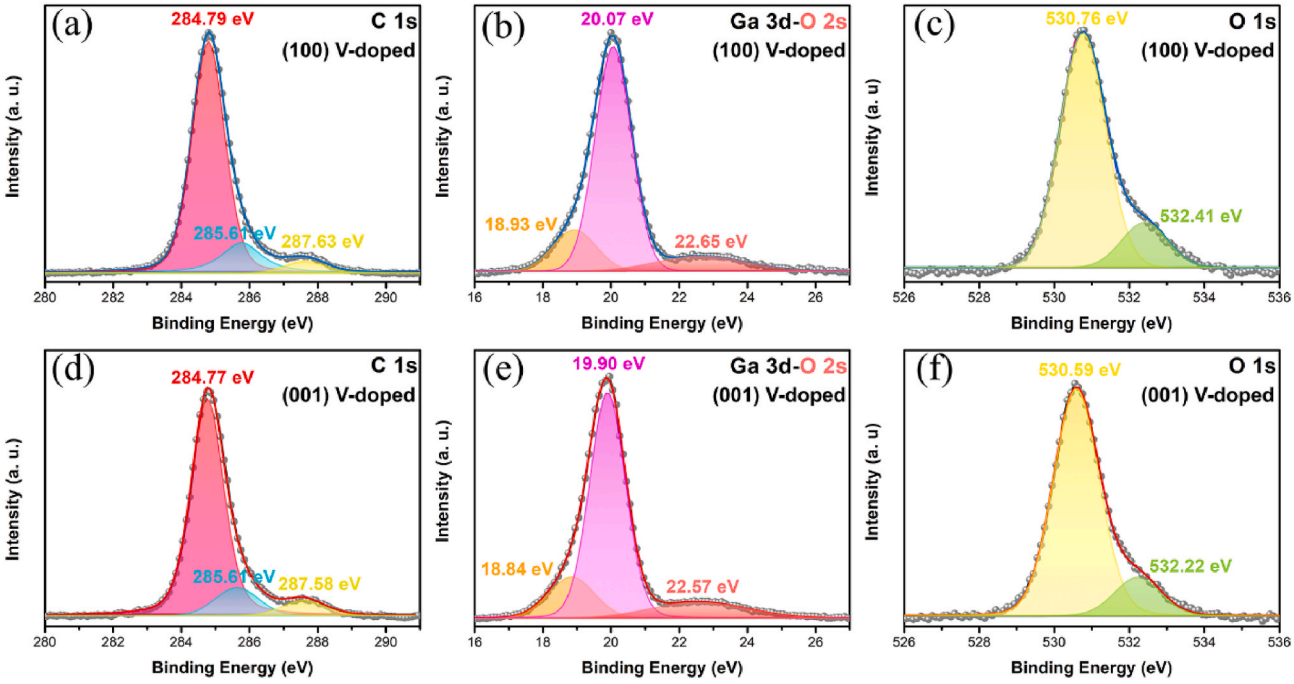


**Fig. 6.** XPS core level of C 1s ((a) and (d)), Ga 3 d-O 2s ((b) and (e)), and O 1s ((c) and (f)) of (100) and (001) V-doped β-$Ga_2O_3$ crystals.

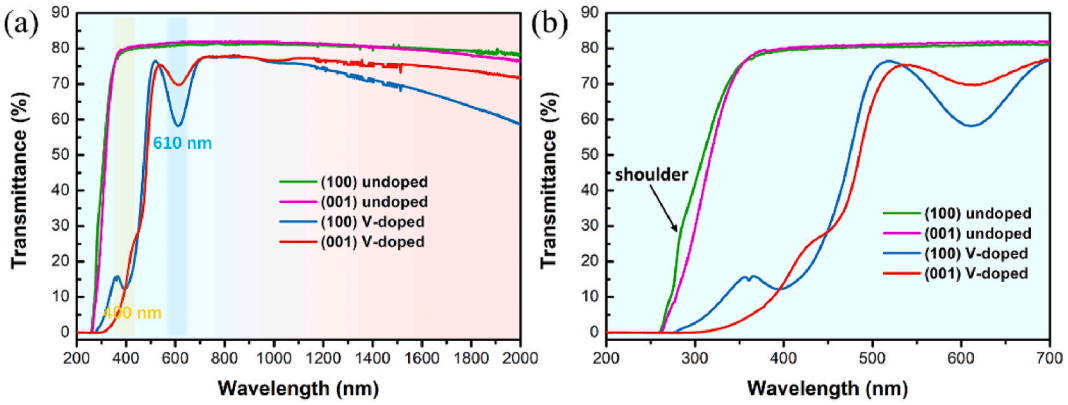


**Fig. 7.** Optical transmittance spectra of the (100) and (001) undoped and V-doped β-$Ga_2O_3$ substrates with the scanning range of (a) 200–2000 nm and (b) 200–700 nm.

(001) substrates. The flat region on the (100) V-doped β-$Ga_2O_3$ substrate partially overlapped with the absorption peak at approximately 400 nm. The ultraviolet cut-off edges of the V-doped (100) and (001) planes showed a red shift compared with that of the undoped sample. This confirms that the optical band gap of the β-$Ga_2O_3$ crystal with V doping also decreased correspondingly, which was due to the defect energy caused by the $V_xO_y$ clusters expanded with increasing of V doping concentration, leading to red shift of the cut-off edge [44]. The cut-off edge of the (001) V-doped β-$Ga_2O_3$ substrate was larger than that of the (100) V-doped β-$Ga_2O_3$ substrate, which was related to the presence of more excess V and defects in the (001) V-doped β-$Ga_2O_3$ crystal.

The Raman spectra of β-$Ga_2O_3$ samples with (100) and (001) planes grown by EFG were recorded at room temperature, as shown in Fig. 8. Ten Raman phonon peaks were observed for each of the (100) and (001) β-$Ga_2O_3$ crystals, which is consistent with the results reported in the literature [27,35]. These Raman peaks are divided into three regions according to the type of vibration modes [53,54]: (I) the low-frequency (less than 250 $cm^{-1}$) modes are related to the oscillation and translational motion of tetrahedral-octahedral chains, (II) the medium-frequency (300−500 $cm^{-1}$) modes originate from the deformation of octahedra, and (III) the high-frequency (above 500 $cm^{-1}$) modes are ascribed to the stretching and bending of tetrahedra. After the introduction of V into the (100) and (001) β-$Ga_2O_3$ crystals, the intensity of the Raman peaks in 300–500 $cm^{-1}$ was significantly weakened (Fig. 8 (a) and (b)), illustrating that V replaced some of the Ga sites in the octahedron (as shown in the insets in Fig. 8 (a) and (b)).

Phonon peaks near 320 $cm^{-1}$ in (II) medium-frequency modes (Fig. 8 (a)) and at approximately 766 $cm^{-1}$ in (III) high-frequency modes (Fig. 8 (b)) were not observed. Moreover, the intensities of the Raman peaks of the two different crystal planes were also different. These discrepancies may be due to the different Ga–O bond interactions in β-$Ga_2O_3$ [27]. Further research is needed to clarify this phenomenon.

### 3.6. Etching and defects observation

Defects on the substrate surface have higher deformation energy, and the areas with higher energy near the surface of the substrate are preferably corroded to form etch pits, whereas a smooth and flat surface remains in the region without defects. To avoid complex corrosion caused by scratches or damage, the β-$Ga_2O_3$ single crystals with different crystal planes were ground and polished under the same processing conditions.

To investigate the defects in the (100) and (001) V-doped β-$Ga_2O_3$ crystals in macroscopic form, the polished substrates were etched simultaneously in phosphoric acid ($H_3PO_4$) at 130 °C for 2 h. The typical etch pits observed for the (100) and (001) V-doped β-$Ga_2O_3$ substrates are shown in Fig. 9. Two types of etch pits were identified: (1) oval-shaped etch pits on the (100) surface, and (2) triangle-shaped etch pits on the (001) surface. Fig. 9(a–c) and (e-g) display the optical microscopy images and 2D and 3D LCM images of the two types of etch pits, respectively. Although these etch pits are randomly distributed, they have a certain directionality. The etch pits with oval shape were similar to those reported by Ohba et al. and Qi et al. [17,36]. The triangular etch pits were analogous to those reported by Kasu et al. and Tao et al. [23,28].

The cross-sectional profiles of the two types of etch pits are shown in Fig. 9(d) and (h). The widths of the etch pits on the (100) and (001) surfaces are approximately 14.0 μm and 19.0 μm, respectively. The depths are approximately 330 nm and 1.2 μm, respectively. These differences are determined to the anisotropy of β-$Ga_2O_3$ crystals belonging

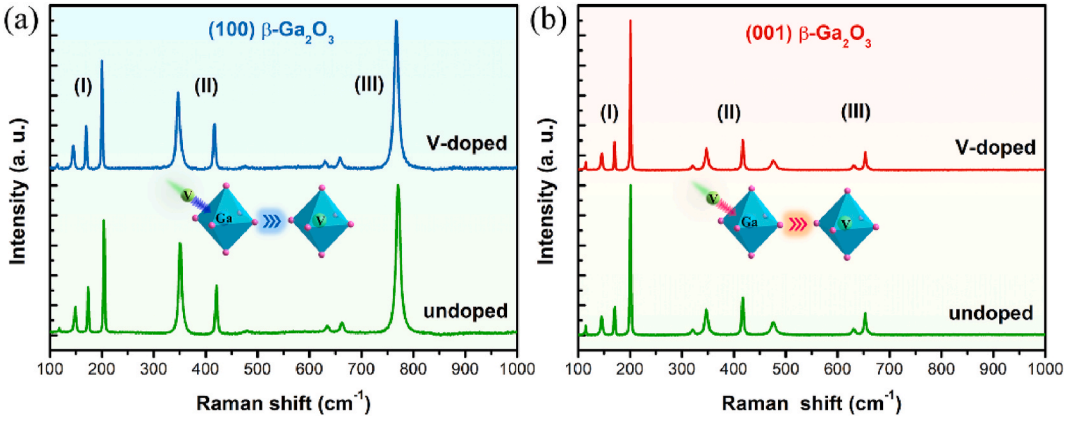


**Fig. 8.** Raman spectra of the (100) (a) and (001) (b) undoped and V-doped β-$Ga_2O_3$ substrates.

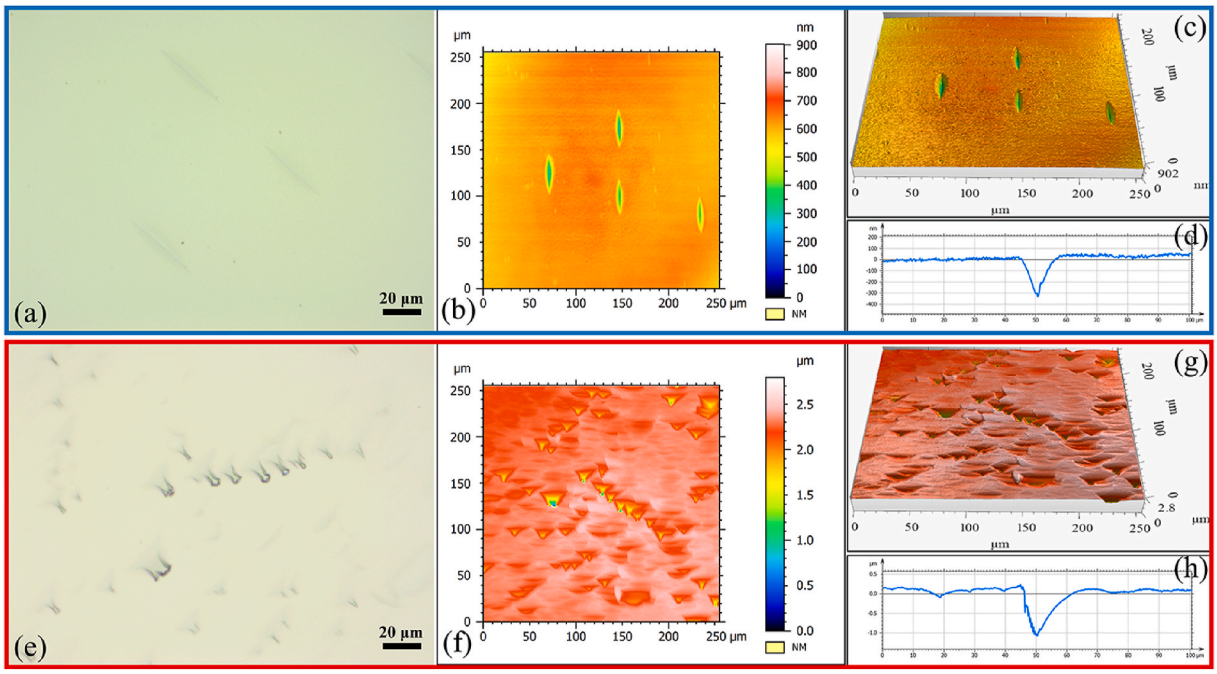


**Fig. 9.** 2D optical micrographs ((a) and (e)) and LCM images ((b) and (f)), 3D LCM images ((c) and (g)) and cross-section curves of the defect pits ((d) and (h)) of the V-doped β-$Ga_2O_3$ substrates on (100) (blue rectangle) and (001) (red rectangle) after chemical etching.

to the monoclinic structure with space group *C*2/*m*. When etching to a certain extent, other facets will also be corroded, and the different corrosion rates of each crystal facet will lead to differences in etch pits. The size of the etch pits formed by dislocations can be altered via extending the etching time, while the shape remains unchanged [17,55]. An increase in the etching time altered the morphology of the etch pits. This implies that the etch pits were caused by void defects [55]. The morphologies of the two types of etch pits (Fig. 9(b) and (f)) did not change after prolonging the etching time, and the size of etch pits at the same positions increased, demonstrating that there were dislocations in the depth direction of these pits. The etch pit densities of the (100) and (001) V-doped β-$Ga_2O_3$ substrates were estimated to be $9.02 \times 10^3$ $cm^{-2}$ and $1.06 \times 10^5$ $cm^{-2}$, respectively. This further proves that there are many dislocation defects in the (001) crystal, which is in well agreement with the results of rocking curves and Hall characterization.

## 4. Conclusions

In conclusion, 0.20 mol% V-doped β-$Ga_2O_3$ crystals with (100) and (001) planes were grown by the EFG technique. The structure, electrical and optical properties, and defects of (100) and (001) V-doped β-$Ga_2O_3$ crystals were comprehensively studied through XRD rocking curves, Hall effects, XPS, optical transmission, Raman spectroscopy, and chemical etching techniques. The (100) V-doped crystal with a small FWHM (43.2 arcsec) and low defect density ($9.02 \times 10^3$ $cm^{-2}$) confirmed the extremely high crystal quality compared to the (001) V-doped crystal. The slight increase in the carrier concentration of the V-doped samples can be interpreted as the formation of $V_xO_y$ clusters as electron trapping traps and the formation of carbon DX centers as compensation acceptors. The flat region in the transmission spectra is related to V doping. Moreover, owing to the anisotropy of the monoclinic structure, the Raman phonon peak strengths of the (100) and (001) V-doped β-$Ga_2O_3$ crystals were different, and the morphologies of the etch pits exhibited oval and triangle shapes, respectively.

## CRediT authorship contribution statement

**Pengkun Li:** Writing – review & editing, Writing – original draft, Software, Methodology, Investigation, Formal analysis, Data curation. **Xueli Han:** Validation, Software, Data curation. **Duanyang Chen:** Writing – review & editing, Data curation. **Qinglin Sai:** Writing – review & editing, Software, Formal analysis. **Hongji Qi:** Supervision, Resources, Funding acquisition.

## Declaration of competing interest

The authors declare that they have no known competing financial interests or personal relationships that could have appeared to influence the work reported in this paper.

## Data availability

Data will be made available on request.

## Acknowledgments

We would like to thank Hangzhou Fujia Gallium Technology Co., Ltd. For their help with the crystal growth, processing and testing. This work was supported by the National Natural Science Foundation of China (grant number 51972319), the Youth Innovation Promotion Association, Chinese Academy of Science (CAS) (grant number 2021245), and the Shanghai Science and Technology Commission (grant number 20511107400).

## References

[1] H. Yang, Z. Xie, G. Li, K. Ou, F. Yu, H. He, H. Wang, X. Yuan, All-dielectric metasurface for fully resolving arbitrary beams on a higher-order Poincaré sphere, Photon. Res. 9 (2021) 331–343, https://doi.org/10.1364/prj.411503.
[2] J. Du, W. Shen, J. Liu, Y. Chen, X. Chen, Z. He, Mode division multiplexing: from photonic integration to optical fiber transmission, Chin. Opt Lett. 19 (2021), 091301, https://doi.org/10.3788/col202119.091301.
[3] R. Xu, X. Ma, Y. Chen, Y. Mei, L. Ying, B. Zhang, H. Long, Effect of oxygen vacancies in heteroepitaxial β-$Ga_2O_3$ thin film solar blind photodetectors, Mater. Sci. Semicond. Process. 144 (2022), 106621, https://doi.org/10.1016/j.mssp.2022.106621.
[4] A. Pandey, Y. Malhotra, P. Wang, K. Sun, X. Liu, Z. Mi, N-polar InGaN/GaN nanowires: overcoming the efficiency cliff of red-emitting micro-LEDs, Photon. Res. 10 (2022) 1107–1116, https://doi.org/10.1364/prj.450465.

[5] H. Yu, Z. Ren, M.H. Memon, S. Fang, D. Wang, Z. Liu, H. Zhang, F. Wu, J. Dai, C. Chen, H. Sun, Cascaded deep ultraviolet light-emitting diode via tunnel junction, Chin. Opt Lett. 19 (2021), 082503, https://doi.org/10.3788/col202119.082503.

[6] R. Pilliadugula, N. Gopalakrishnan, Room temperature ammonia sensing performances of pure and Sn doped β-$Ga_2O_3$, Mater. Sci. Semicond. Process. 135 (2021), 106086, https://doi.org/10.1016/j.mssp.2021.106086.

[7] M. Zhang, H. Chen, J. Yin, J. Wang, J. Wang, P. Yan, Recent development of saturable absorbers for ultrafast lasers, Chin. Opt Lett. 19 (2021), 081405, https://doi.org/10.3788/col202119.081405.

[8] S.J. Pearton, J. Yang, P.H. Cary, F. Ren, J. Kim, M.J. Tadjer, M.A. Mastro, A review of $Ga_2O_3$ materials, processing, and devices, Appl. Phys. Rev. 5 (2018), 011301, https://doi.org/10.1063/1.5006941.

[9] X. Hou, Y. Zou, M. Ding, Y. Qin, Z. Zhang, X. Ma, P. Tan, S. Yu, X. Zhou, X. Zhao, G. Xu, H. Sun, S. Long, Review of polymorphous $Ga_2O_3$ materials and their solar-blind photodetector applications, J. Phys. D Appl. Phys. 54 (2020), 043001, https://doi.org/10.1088/1361-6463/abbb45.

[10] R. Singh, T.R. Lenka, D.K. Panda, R.T. Velpula, B. Jain, H.Q.T. Bui, H.P.T. Nguyen, The dawn of $Ga_2O_3$ HEMTs for high power electronics - a review, Mater. Sci. Semicond. Process. 119 (2020), 105216, https://doi.org/10.1016/j.mssp.2020.105216.

[11] S.-Y. Chu, T.-H. Yeh, C.-T. Lee, H.-Y. Lee, Mg-doped beta-$Ga_2O_3$ films deposited by plasma-enhanced atomic layer deposition system for metal-semiconductor-metal ultraviolet C photodetectors, Mater. Sci. Semicond. Process. 142 (2022), 106471, https://doi.org/10.1016/j.mssp.2022.106471.

[12] H. Cui, H.F. Mohamed, C. Xia, Q. Sai, W. Zhou, H. Qi, J. Zhao, J. Si, X. Ji, Tuning electrical conductivity of β-$Ga_2O_3$ single crystals by Ta doping, J. Alloys Compd. 788 (2019) 925–928, https://doi.org/10.1016/j.jallcom.2019.02.076.

[13] B. Wang, D. Look, G. Farlow, Optical and electrical properties of Ti-doped β-$Ga_2O_3$ ($Ti^{3+}$:β-$Ga_2O_3$) bulk crystals grown by floating zone method, J. Phys. D Appl. Phys. 53 (2020), 444001, https://doi.org/10.1088/1361-6463/aba3eb.

[14] Z. Galazka, R. Uecker, D. Klimm, K. Irmscher, M. Naumann, M. Pietsch, A. Kwasniewski, R. Bertram, S. Ganschow, M. Bickermann, Scaling-up of bulk β-$Ga_2O_3$ single crystals by the Czochralski method, ECS J. Solid State Sci. Technol. 6 (2017) Q3007–Q3011, https://doi.org/10.1149/2.0021702jss.

[15] Z. Galazka, S. Ganschow, A. Fiedler, R. Bertram, D. Klimm, K. Irmscher, R. Schewski, M. Pietsch, M. Albrecht, M. Bickermann, Doping of Czochralski-grown bulk β-$Ga_2O_3$ single crystals with Cr, Ce and Al, J. Cryst. Growth 486 (2018) 82–90, https://doi.org/10.1016/j.jcrysgro.2018.01.022.

[16] K. Hoshikawa, E. Ohba, T. Kobayashi, J. Yanagisawa, C. Miyagawa, Y. Nakamura, Growth of β-$Ga_2O_3$ single crystals using vertical Bridgman method in ambient air, J. Cryst. Growth 447 (2016) 36–41, https://doi.org/10.1016/j.jcrysgro.2016.04.022.

[17] E. Ohba, T. Kobayashi, T. Taishi, K. Hoshikawa, Growth of (100), (010) and (001) β-$Ga_2O_3$ single crystals by vertical Bridgman method, J. Cryst. Growth 556 (2021), 125990, https://doi.org/10.1016/j.jcrysgro.2020.125990.

[18] H. Aida, K. Nishiguchi, H. Takeda, N. Aota, K. Sunakawa, Y. Yaguchi, Growth of β-$Ga_2O_3$ Single Crystals by the edge-defined, film fed growth method, Jpn. J. Appl. Phys. 47 (2008) 8506–8509, https://doi.org/10.1143/JJAP.47.8506.

[19] B. Fu, G. Jian, W. Mu, Y. Li, H. Wang, Z. Jia, Y. Li, S. Long, Y. Shi, X. Tao, Crystal growth and design of Sn-doped β-$Ga_2O_3$: morphology, defect and property studies of cylindrical crystal by EFG, J. Alloys Compd. 896 (2022), 162830, https://doi.org/10.1016/j.jallcom.2021.162830.

[20] E. Villora, K. Shimamura, Y. Yoshikawa, K. Aoki, N. Ichinose, Large-size β-$Ga_2O_3$ single crystals and wafers, J. Cryst. Growth 270 (2004) 420–426, https://doi.org/10.1016/j.jcrysgro.2004.06.027.

[21] E. Ohba, T. Kobayashi, M. Kado, K. Hoshikawa, Defect characterization of β-$Ga_2O_3$ single crystals grown by vertical Bridgman method, Jpn. J. Appl. Phys. 55 (2016), 1202BF, https://doi.org/10.7567/jjap.55.1202bf.

[22] D.J. Rogers, D.C. Look, F.H. Teherani, S. Yamakoshi, T. Masui, Y. Yamaoka, S. Watanabe, K. Koshi, A. Kuramata, Bulk crystal growth of $Ga_2O_3$, OXIDE-BASED MATERIALS AND DEVICES IX, UNSP 105330E, https://doi.org/10.1117/12.2301405, 2018.

[23] B. Fu, W. Mu, J. Zhang, X. Wang, W. Zhuang, Y. Yin, Z. Jia, X. Tao, A study on the technical improvement and the crystalline quality optimization of columnar β-$Ga_2O_3$ crystal growth by an EFG method, CrystEngComm 22 (2020) 5060–5066, https://doi.org/10.1039/d0ce00683a.

[24] Z. Guo, A. Verma, X. Wu, F. Sun, A. Hickman, T. Masui, A. Kuramata, M. Higashiwaki, D. Jena, T. Luo, Anisotropic thermal conductivity in single crystal β-gallium oxide, Appl. Phys. Lett. 106 (2015), 111909, https://doi.org/10.1063/1.4916078.

[25] M. Schubert, R. Korlacki, S. Knight, T. Hofmann, S. Schöche, V. Darakchieva, E. Janzén, B. Monemar, D. Gogova, Q.T. Thieu, R. Togashi, H. Murakami, Y. Kumagai, K. Goto, A. Kuramata, S. Yamakoshi, M. Higashiwaki, Anisotropy, phonon modes, and free charge carrier parameters in monoclinic β-gallium oxide single crystals, Phys. Rev. B 93 (2016), 125209, https://doi.org/10.1103/PhysRevB.93.125209.

[26] W. Mu, Z. Jia, Y. Yin, Q. Hu, Y. Li, B. Wu, J. Zhang, X. Tao, High quality crystal growth and anisotropic physical characterization of β-$Ga_2O_3$ single crystals grown by EFG method, J. Alloys Compd. 714 (2017) 453–458, https://doi.org/10.1016/j.jallcom.2017.04.185.

[27] K. Zhang, Z. Xu, S. Zhang, H. Wang, H. Cheng, J. Hao, J. Wu, F. Fang, Raman and photoluminescence properties of un-/ion-doped β-$Ga_2O_3$ single-crystals prepared by edge-defined film-fed growth method, Physica B 600 (2021), 412624, https://doi.org/10.1016/j.physb.2020.412624.

[28] M. Kasu, T. Oshima, K. Hanada, T. Moribayashi, A. Hashiguchi, T. Oishi, K. Koshi, K. Sasaki, A. Kuramata, O. Ueda, Crystal defects observed by the etch-pit method and their effects on Schottky-barrier-diode characteristics on (-201) β-$Ga_2O_3$, Jpn. J. Appl. Phys. 56 (2017), 091101, https://doi.org/10.7567/jjap.56.091101.

[29] T. Oshima, A. Hashiguchi, T. Moribayashi, K. Koshi, K. Sasaki, A. Kuramata, O. Ueda, T. Oishi, M. Kasu, Electrical properties of Schottky barrier diodes fabricated on (001) β-$Ga_2O_3$ substrates with crystal defects, Jpn. J. Appl. Phys. 56 (2017), 086501, https://doi.org/10.7567/jjap.56.086501.

[30] A. Kuramata, K. Koshi, S. Watanabe, Y. Yamaoka, T. Masui, S. Yamakoshi, High-quality β-$Ga_2O_3$ single crystals grown by edge-defined film-fed growth, Jpn. J. Appl. Phys. 55 (2016), 1202A1202, https://doi.org/10.7567/jjap.55.1202a2.

[31] W. Zhou, C. Xia, Q. Sai, H. Zhang, Controlling n-type conductivity of β-$Ga_2O_3$ by Nb doping, Appl. Phys. Lett. 111 (2017), 242103, https://doi.org/10.1063/1.4994263.

[32] A. Luchechko, V. Vasyltsiv, Y. Zhydachevskyy, M. Kushlyk, S. Ubizskii, A. Suchocki, Luminescence spectroscopy of $Cr^{3+}$ ions in bulk single crystalline β-$Ga_2O_3$, J. Phys. D Appl. Phys. 53 (2020), 354001, https://doi.org/10.1088/1361-6463/ab8c7d.

[33] V. Vasyltsiv, A. Luchechko, Y. Zhydachevskyy, L. Kostyk, R. Lys, D. Slobodzyan, R. Jakieła, B. Pavlyk, A. Suchocki, Correlation between electrical conductivity and luminescence properties in β-$Ga_2O_3$:$Cr^{3+}$ and β-$Ga_2O_3$:Cr,Mg single crystals, J. Vac. Sci. Technol., A 39 (2021), 033201, https://doi.org/10.1116/6.0000859.

[34] J. Huang, Y. Hu, T. Zou, K. Tang, Z. Zhang, Y. Ma, B. Li, L. Wang, Y. Lu, Investigation of properties of transparent and conducting V-doped $Ga_2O_3$ films, Surf. Coating. Technol. 366 (2019) 70–74, https://doi.org/10.1016/j.surfcoat.2018.12.130.

[35] P. Li, X. Han, D. Chen, Q. Sai, H. Qi, Effect of air annealing on the structural, electrical, and optical properties of V-doped β-$Ga_2O_3$ single crystals, J. Alloys Compd. 908 (2022), 164590, https://doi.org/10.1016/j.jallcom.2022.164590.

[36] P. Li, Y. Bu, D. Chen, Q. Sai, H. Qi, Investigation of the crack extending downward along the seed of the β-$Ga_2O_3$ crystal grown by the EFG method, CrystEngComm 23 (2021) 6300–6306, https://doi.org/10.1039/d1ce00576f.

[37] P. Li, X. Han, D. Chen, Q. Sai, H. Qi, Controllability of β-$Ga_2O_3$ single crystal conductivity by V doping, CrystEngComm 24 (2022) 5588–5596, https://doi.org/10.1039/d2ce00418f.

[38] K. Yamaguchi, First principles study on electronic structure of β-$Ga_2O_3$, Solid State Commun. 131 (2004) 739–744, https://doi.org/10.1016/j.ssc.2004.07.030.

[39] S. Mu, M. Wang, J.B. Varley, J.L. Lyons, D. Wickramaratne, C.G. Van de Walle, Role of carbon and hydrogen in limiting n-type doping of monoclinic $(Al_xGa_{1-x})_2O_3$, Phys. Rev. B 105 (2022), 155201, https://doi.org/10.1103/PhysRevB.105.155201.

[40] J.L. Lyons, D. Steiauf, A. Janotti, C.G. Van de Walle, Carbon as a shallow donor in transparent conducting oxides, Phys. Rev. Appl. 2 (2014), 064005, https://doi.org/10.1103/PhysRevApplied.2.064005.

[41] M.J. Tadjer, J.L. Lyons, N. Nepal, J.A. Freitas Jr., A.D. Koehler, G.M. Foster, Review—theory and characterization of doping and defects in β-$Ga_2O_3$, ECS J. Solid State Sc. 8 (2019) Q3187–Q3194, https://doi.org/10.1149/2.0341907jss.

[42] H. Liu, W. Zhu, D. Long, J. Zhu, G. Pezzotti, Porous $V_2O_5$ nanorods/reduced graphene oxide composites for high performance symmetric supercapacitors, Appl. Surf. Sci. 478 (2019) 383–392, https://doi.org/10.1016/j.apsusc.2019.01.273.

[43] H. Cui, Q. Sai, H. Qi, J. Zhao, J. Si, M. Pan, Analysis on the electronic trap of β-$Ga_2O_3$ single crystal, J. Mater. Sci. 54 (2019) 12643–12649, https://doi.org/10.1007/s10853-019-03777-1.

[44] N. Zhang, H. Liu, Q. Sai, C. Shao, C. Xia, L. Wan, Z.C. Feng, H.F. Mohamed, Structural and electronic characteristics of Fe-doped β-$Ga_2O_3$ single crystals and the annealing effects, J. Mater. Sci. 56 (2021) 13178–13189, https://doi.org/10.1007/s10853-021-06027-5.

[45] S. Lany, Defect phase diagram for doping of $Ga_2O_3$, Apl. Mater. 6 (2018), 046103, https://doi.org/10.1063/1.5019938.

[46] R. Carli, C.L. Bianchi, XPS analysis of gallium oxides, Appl. Surf. Sci. 74 (1994) 99–102, https://doi.org/10.1016/0169-4332(94)90104-X.

[47] A. Navarro-Quezada, S. Alamé, N. Esser, J. Furthmüller, F. Bechstedt, Z. Galazka, D. Skuridina, P. Vogt, Near valence-band electronic properties of semiconducting β-$Ga_2O_3$ (100) single crystals, Phys. Rev. B 92 (2015), 195306, https://doi.org/10.1103/PhysRevB.92.195306.

[48] V. Janakiraman, V. Tamilnayagam, R.S. Sundararajan, S. Suresh, C.S. Biju, Structural and optical properties of pure $SnO_2$ and $V_2O_5$/$SnO_2$ nanocomposite thin films for gas sensing application, J. Mater. Sci. Mater. Electron. 31 (2020) 15477–15488, https://doi.org/10.1007/s10854-020-04110-2.

[49] Y. Berencén, Y. Xie, M. Wang, S. Prucnal, L. Rebohle, S. Zhou, Structural and optical properties of pulsed-laser deposited crystalline β-$Ga_2O_3$ thin films on silicon, Semicond. Sci. Technol. 34 (2019), 035001, https://doi.org/10.1088/1361-6641/aafc90.

[50] H.H. Tippins, Optical absorption and photoconductivity in the band edge of β-$Ga_2O_3$, Phys. Rev. 140 (1965) A316–A319, https://doi.org/10.1103/PhysRev.140.A316.

[51] H. Tang, N. He, Z. Zhu, M. Gu, B. Liu, J. Xu, M. Xu, L. Chen, J. Liu, X. Ouyang, Temperature-dependence of X-ray excited luminescence of β-$Ga_2O_3$ single crystals, Appl. Phys. Lett. 115 (2019), 071904, https://doi.org/10.1063/1.5110535.

[52] W. Mu, X. Chen, G. He, Z. Jia, J. Ye, B. Fu, J. Zhang, S. Ding, X. Tao, Anisotropy and in-plane polarization of low-symmetrical β-$Ga_2O_3$ single crystal in the deep ultraviolet band, Appl. Surf. Sci. 527 (2020), 146648, https://doi.org/10.1016/j.apsusc.2020.146648.

[53] T. Onuma, S. Fujioka, T. Yamaguchi, Y. Itoh, M. Higashiwaki, K. Sasaki, T. Masui, T. Honda, Polarized Raman spectra in β-$Ga_2O_3$ single crystals, J. Cryst. Growth 401 (2014) 330–333, https://doi.org/10.1016/j.jcrysgro.2013.12.061.
[54] S. Mandal, K. Arts, H.C.M. Knoops, J.A. Cuenca, G.M. Klemencic, O.A. Williams, Surface zeta potential and diamond growth on gallium oxide single crystal, Carbon 181 (2021) 79–86, https://doi.org/10.1016/j.carbon.2021.04.100.
[55] K. Hanada, T. Moribayashi, K. Koshi, K. Sasaki, A. Kuramata, O. Ueda, M. Kasu, Origins of etch pits in β-$Ga_2O_3$ (010) single crystals, Jpn. J. Appl. Phys. 55 (2016), 1202BG, https://doi.org/10.7567/jjap.55.1202bg.